

# Simulation and optimization of liquid crystal gratings with alternate twisted nematic and planar aligned regions

Jia-Nan Li,<sup>1</sup> Xi-Kui Hu,<sup>1,2</sup> Bing-Yan Wei,<sup>1</sup> Zi-Jian Wu,<sup>1</sup> Shi-Jun Ge,<sup>1</sup> Wei Ji,<sup>1</sup>  
Wei Hu,<sup>1,\*</sup> and Yan-Qing Lu<sup>1,3</sup>

<sup>1</sup>National Laboratory of Solid State Microstructures and College of Engineering and Applied Sciences,  
Nanjing University, Nanjing 210093, China

<sup>2</sup>College of Mathematics and Physics, Chongqing University of Posts and Telecommunications,  
Chongqing 400065, China

<sup>3</sup>e-mail: yqlu@nju.edu.cn

\*Corresponding author: huwei@nju.edu.cn

Received 4 March 2014; revised 18 April 2014; accepted 26 April 2014;  
posted 28 April 2014 (Doc. ID 207473); published 29 May 2014

Electro-optical properties of liquid crystal (LC) gratings with alternate twisted nematic (TN) and planar aligned (PA) regions are simulated. Three typical steps are introduced: first, the LC director distributions of the two different regions are simulated. Then, the phase and amplitude of the emergent light in each region are calculated through Jones matrix. Based on this information, the voltage-dependent diffraction efficiency is achieved by Fourier transformation, finally. It gives an exact explanation for the mechanism of this kind of gratings. Experiments with optimized parameters are carried out through photopatterning. The trend of the measured voltage-dependent efficiency fits the simulation result very well. This method can be used to optimize the performance of LC gratings with alternate TN and PA regions, and exhibits great potential in the simulation of corresponding photonics and display applications. © 2014 Optical Society of America

*OCIS codes:* (160.3710) Liquid crystals; (050.1950) Diffraction gratings.

<http://dx.doi.org/10.1364/AO.53.000E14>

## 1. Introduction

A lot of attention has been focused on electrically tunable liquid crystal (LC) gratings in the areas of optical switches, beam steering, and optical waveguides for its advantages of high definition, light weight, no moving parts, and low power consumption [1–5]. LC gratings can be achieved by the realization of a periodical distribution of the refractive index profile. There are mainly three strategies applied to fabricate LC gratings. The first is to form a periodical LC molecular distribution inside the gratings

by utilizing the natural properties of LC materials or holographic recording in polymer-dispersed LCs [6–9]. The second is to generate a periodical electric field through patterned electrodes [10–14] to form LC gratings. The third is to guide LC directors through periodically patterned alignment layers by conventional mechanical rubbing [15,16] or noncontact photoalignment techniques [4,17–21]. Among all the above methods, photoalignment has been widely used for the advantages of easy fabrication, no mechanical pollution, and re-configurability.

By means of a two-step exposure photoalignment, we demonstrated a kind of LC grating with alternate twisted nematic (TN) and planar aligned (PA) regions in one cell [18]. Thanks to its unique structure,

---

1559-128X/14/220E14-05\$15.00/0

© 2014 Optical Society of America

a four-state feature of transmittance and a low operation voltage can be obtained. It can be switched in a small voltage interval of 0.15 V only to voltage values below 1 V, exhibiting great potential in low-power-consumption devices such as optical switches and electro-optic logic gates. More recently, TN/PA LC fork gratings with dislocations at the center have been introduced for generating optical vortices [22]. In the above cases, we attributed the diffraction to the combination of alternate phase and amplitude modulation. However, the performance-related parameters and the contribution by amplitude and phase modulation along with tuning of the applied voltage are still unclear. The clarification of the mechanism will facilitate the performance optimization of this type of gratings. It will benefit the design of novel optical devices as well.

In this work, we simulated the LC director distribution of TN and PA regions in gratings by the commercial software TechWiz LCD. Then the phase and amplitude of the emergent light in each region were calculated through Jones matrix. Subsequently, the voltage-dependent diffraction efficiency of the first order was achieved by Fourier transformation according to the emergent light wavefront. We adjusted the corresponding parameters to improve the performance. Experiments with optimized parameters were carried out, and both the efficiency and the dynamic range increased evidently, and the results fit the simulation very well.

## 2. Theory and Simulation

The grating's configuration is presented in Fig. 1. It exhibits one period of adjacent TN and PA regions. As shown, in the TN region, the LC directors are twisted by 90° continuously from the incident side toward the emergent side, whereas the alignment direction in the PA region is 45° with respect to both the polarizer and the analyzer. The incident polarization is parallel to the LC orientation in the TN region on the bottom substrate.

LCs exhibit good fluidity and their director distributions under an applied field could be obtained by continuum theory. TechWiz LCD is commercial software utilizing the finite-element method to solve such problems, which is used widely for simulation of LC director distributions. In our work, we use this

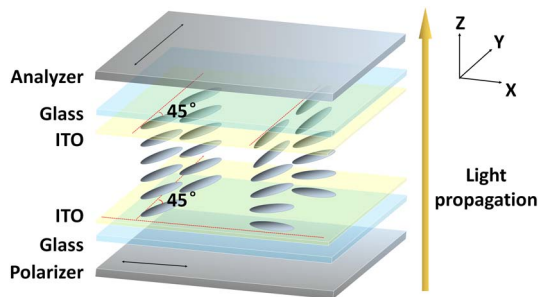


Fig. 1. Scheme of LC orientations in TN/PA gratings; the yellow arrow represents light propagation, whereas the black double-headed arrows indicate transmitted polarization.

software to calculate the LC director distributions separately in the TN and PA regions. The anchoring energy is set to be strong according to our experiment and the tilt angle is 2°. The LC layer is separated into 50 layers. Cell gaps vary from 4 to 8 μm with an interval of 0.1 μm. The LC in the TN regions is twisted 90°. E7 ( $n_e = 1.7429$ ,  $n_o = 1.5198$ ) is adopted here for the simulation. By this means, the tilt angle and azimuth angle can be obtained for each layer.

Then we utilized Jones matrix methods to get the output wavefront of the TN and PA regions. In our work, light is incident normally on the grating. The grating constant ( $\Lambda$ ) is much larger than the wavelength ( $\lambda$ ; here  $\lambda = 632.8$  nm); therefore, the light interference inside the grating can be neglected and the periodical boundary condition can be applied here. For the LC has been divided into many layers, the difference of refractive index between adjacent LC layers is small enough to neglect the reflection. Based on the above assumptions, the Jones matrix method could be applied here.

The polarization direction of the incident light was defined as the  $x$  direction and the analyzer's polarization direction was set as  $y$  direction. The Jones vector ( $J$ ) of the incident light is  $J_0 = (1, 0)$ . In our work, the LC was split into 50 layers. Each layer can be considered as a wave plate that is represented as a Jones matrix ( $W$ ). According to the director distribution carried out previously through TechWiz simulation, the effective refractive index and phase retardation of ordinary and extraordinary rays after traversing through each layer could be determined. Therefore, the Jones vector of the emergent light is the product of the overall Jones matrix ( $M$ ) and  $J_0$ :

$$J = MJ_0, \quad (1)$$

where

$$M = R'_n W_n R_n \dots R'_2 W_2 R_2 R'_1 W_1 R_1, \quad (2)$$

where

$$R_n = \begin{pmatrix} \cos \psi & \sin \psi \\ -\sin \psi & \cos \psi \end{pmatrix}, \quad (3)$$

$$W = \begin{pmatrix} e^{-i2\pi n_{\text{eff}}(z)d/\lambda} & 0 \\ 0 & e^{-i2\pi n_o d/\lambda} \end{pmatrix}. \quad (4)$$

$R_n$  represents the coordinate rotation matrix of the  $n$ th layer. In each LC layer,  $\psi$  is defined as the azimuthal angle between the incident polarization direction and the fast axis of each wave plate.  $R'_n$  represents the transpose of  $R_n$ .  $n_{\text{eff}}(z)$  is the effective index of the layer at  $z$  position:

$$n_{\text{eff}}(z) = \frac{n_e n_o}{\sqrt{n_e^2 (\sin \theta)^2 + n_o^2 (\cos \theta)^2}}, \quad (5)$$

where  $\theta$  represents the corresponding tilt angle.

Here, both amplitude and phase are included in the Jones vector of the emergent light. The analyzer is set in the  $y$  direction; therefore, only the  $y$ -component of the output Jones vector is taken into account. In Fig. 2(a), the green curve is the voltage-dependent output amplitude ( $y$ -component) in the TN regions, whereas the red curve represents that in the PA regions. The grating is based on the combination of amplitude and phase modulation, except for several specific cases: (i) when the applied voltage is 0.71 V, the transmission of the TN and PA regions reaches 100% simultaneously; thus, the grating is a pure phase grating and the PA regions work as a half-wave plate; (ii) when the applied voltage is 0.55 and 0.92 V, the transmission of the PA regions approaches 0; thus, the grating turns to a pure amplitude grating; and (iii) as can be speculated, when a saturated voltage is applied, a uniform homeotropic state is formed; thus, an off state is achieved. The green curve in Fig. 2(b) represents the voltage-dependent phase shift of the output light through the analyzer in the TN regions. It varies from  $-\pi$  to  $\pi$ , as a relative phase change is considered. That indicates that the phase change is continuous. The red curve in Fig. 2(b) reveals the phase shift of the output light in the PA regions. The phase changes

abruptly by one  $\pi$  at 0.55 and 0.92 V, corresponding to the two zero points in amplitude as presented in Fig. 2(a). In these conditions, the PA domain works as a full-wave plate. And the two abrupt phase changes of  $\pi$  can be attributed to the fact that the oscillation direction of the electric field reverses when the amplitude is zero. Whereas for the TN regions, no zero point in amplitude exists before the saturation voltage, and the phase change is continuous. Thus, the phase difference ( $\Delta\varphi$ ) between the TN and PA regions changes discontinuously with the applied voltage, resulting in a sharp change of  $\cos(\Delta\varphi)$  as shown in Fig. 2(c).

Based on the output wavefront of adjacent TN and PA domains, further calculation can be carried out on the diffraction efficiency. Fourier transformation is utilized to calculate the diffraction efficiency (defined as the ratio of the intensity of a certain diffraction order to that of the total input light) of the LC grating. For a 1D grating, the electric ( $E_1$ ) and optical ( $I_1$ ) intensity of the first-order diffraction can be calculated as

$$E_1 = \frac{1}{\Lambda} \int_0^\Lambda A e^{i\varphi(x)} e^{\frac{i2\pi x}{\Lambda}} dx$$

$$= \frac{1}{i2\pi} (e^{i2\pi r} - 1) \times (A_{PA} e^{i\varphi_{PA}} - A_{TN} e^{i\varphi_{TN}}), \quad (6)$$

$$I_1 = |E_1|^2$$

$$= \left| \frac{1}{i2\pi} (e^{i2\pi r} - 1) \right|^2 (A_{PA}^2 + A_{TN}^2 - 2A_{PA}A_{TN} \cos \Delta\varphi); \quad (7)$$

$\varphi(x)$  represents the phase of the emergent light at  $x$  point.  $\varphi_{PA}$ ,  $\varphi_{TN}$ ,  $A_{PA}$ , and  $A_{TN}$  represent the phase and amplitude of the emergent light in the PA and TN regions, respectively.  $\Delta\varphi$  is the difference between  $\varphi_{PA}$  and  $\varphi_{TN}$ . According to Eq. (7), the maximum diffraction coefficient exists when  $r = 0.5$ , indicating that the widths of the PA and TN regions are equal in each period.

The simulation results of the dependence of diffraction efficiency on cell gap and applied voltage are shown in Fig. 3. The red part represents higher diffraction efficiency, whereas the blue part represents lower diffraction efficiency.

According to Eq. (7), two factors affect the first-order diffraction efficiency simultaneously. One is the amplitude of the emergent light in the TN and PA regions, and the other is the phase difference between them. When the cell gap is 4.3 or 7.5  $\mu\text{m}$ , diffraction efficiency appears to be around 0 without an applied voltage. It is ascribed to the fact that the phase difference between the emergent light in the TN and PA region is an integral multiple of  $2\pi$ , and the amplitude of the two regions equals each other. To achieve high diffraction efficiency, the

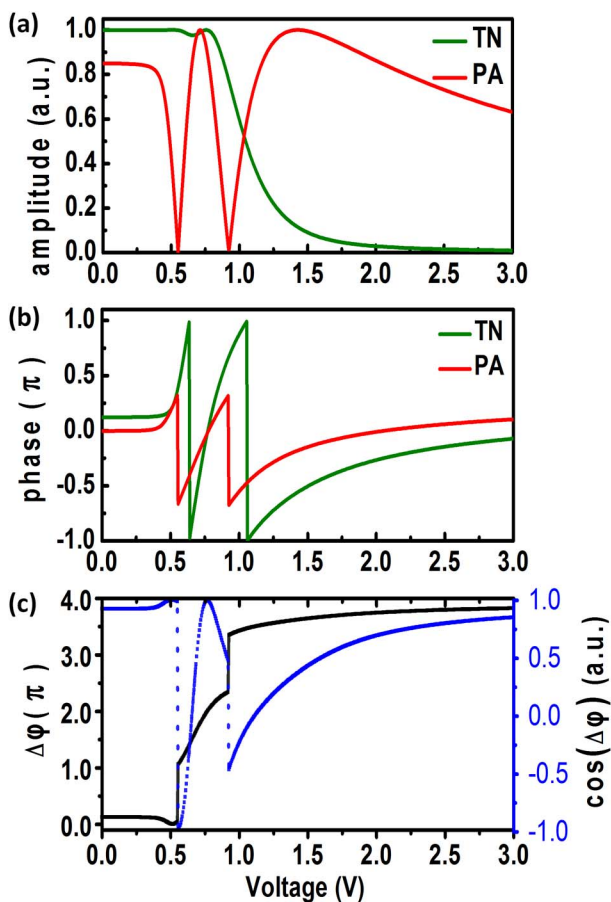


Fig. 2. Voltage-dependent (a) amplitude and (b) phase of TN and PA regions. (c) Voltage-dependent phase difference ( $\Delta\varphi$ ) between adjacent TN and PA regions, and its cosine value. Cell gap is 6  $\mu\text{m}$ .

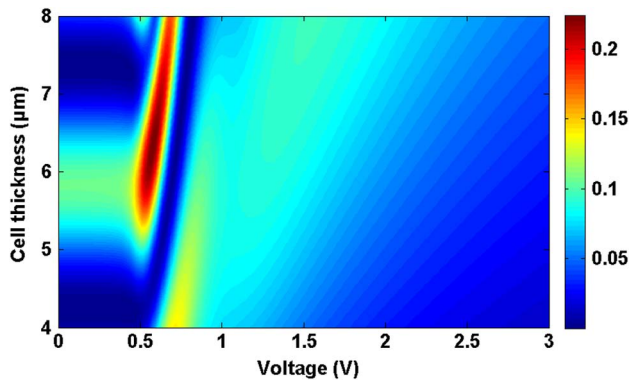


Fig. 3. Simulation result of cell gap-dependent diffraction efficiency of the first order in the applied voltage range from 0 to 3 V.

amplitude of both TN and PA regions should reach maximum at the same time, and their phase difference should be odd multiples of  $\pi$ . From the simulation, the maximum diffraction efficiency can reach 20% when the cell gap is around 6  $\mu\text{m}$ . By increasing the voltage slightly by about 0.15 V, the diffraction efficiency could be suppressed highly. We attribute it to the reasons below. The value of  $\cos(\Delta\varphi)$  reaches  $-1$  at about 0.6 V as in Fig. 2(c). The minimum value of  $\cos(\Delta\varphi)$  permits high diffraction efficiency according to Eq. (7). After increasing the applied voltage slightly,  $\cos(\Delta\varphi)$  reaches 1 at 0.75 V and the amplitude of the TN and PA regions reaches maximum simultaneously, leading to an off state of the grating according to Eq. (7). This characteristic permits a wide dynamic range in a very small interval at a low operation voltage.

### 3. Experiments and Discussion

Optimized parameters based on the simulation were introduced into our experiments to obtain a high-performance grating. The same LC E7 is used in our experiments. A cell gap of 6.3  $\mu\text{m}$  is chosen in order to achieve maximum diffraction efficiency. The grating constant ( $\Lambda$ ) is 50  $\mu\text{m}$  and the duty cycle is 50%.

SD1 (Dai-Nippon Ink and Chemicals, Japan) was utilized as the alignment layer to achieve the desired LC director distribution. Under UV exposure, SD1 molecules tend to reorient their absorption oscillators perpendicular to the UV light polarization direction. And the orientation of SD1 will spread to adjacent LC molecules, thus guiding the LC directors. We dissolved SD1 in *N,N*-dimethylformamide at a concentration of 0.5 wt. %. The solution was spin-coated on indium-tin oxides (ITO)-coated glass substrates. Two substrates were set perpendicular to each other under linearly polarized light to achieve an exposure dose of ca. 5  $\text{J}/\text{cm}^2$ . The polarization direction of the exposure light is parallel to one side of the substrates. By assembling two substrates, a 90° TN cell was formed. After that, the cell was exposed again utilizing a digital micro-mirror device (DMD)-based microlithography system [23] to form another alignment direction 45° with respect

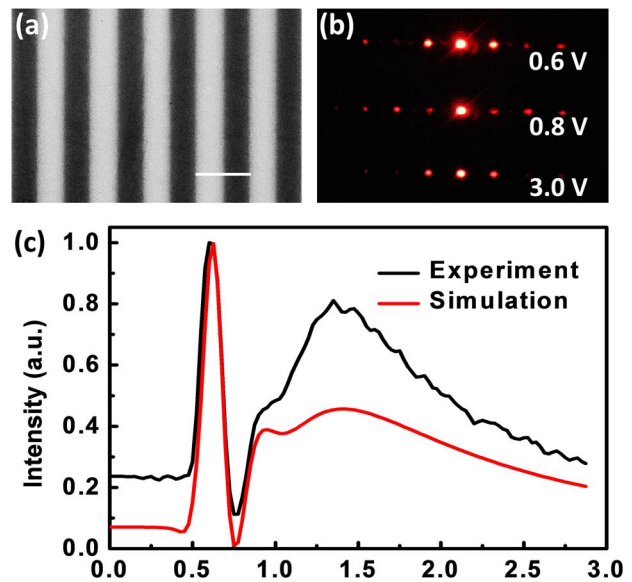


Fig. 4. (a) Micrograph of the grating under crossed polarizers; the scale bar is 50  $\mu\text{m}$ . (b) Diffraction patterns under different voltages. (c) Simulation and experimental results of first-order intensity versus applied voltage.

to the previous alignment direction. The regions exposed for a second time were realigned to be PA, whereas regions only exposed once remained to be TN alignment. Thus, a cell with alternate PA and TN regions was constructed. After E7 was infiltrated into the cell, the cell was observed under a polarization microscope.

The pattern in Fig. 4(a) is due to different transmittance in the TN and PA regions under crossed polarizers. The widths of the alternate TN and PA stripes are 25  $\mu\text{m}$ . The uniform brightness in the same regions (TN or PA) and a good replication of the pattern exhibit the high quality of the gratings. To compare with the simulation results, the electro-optical properties of the gratings were tested.

1 kHz rectangular signals with a duty cycle of 50% were applied on our samples. A He-Ne laser ( $\lambda = 632.8 \text{ nm}$  at 25°C) was incident normally on the cell to generate diffraction patterns. The intensity of the first order was recorded by a photodetector. Figure 4(b) shows the diffraction patterns under different voltages. Figure 4(c) reveals the simulation and experimental results of the voltage-dependent intensity of the first order.

As we can see, the diffraction efficiency does not change under the threshold voltage (0.45 V). Over the threshold, the efficiency changes as a result of combined phase and amplitude modulation. When voltage increases, the diffraction efficiency reaches maximum ( $\sim 20\%$ ) at 0.6 V, and another shoulder peak appears at around 1 V. The featured sharp and shoulder peaks between 0.45 and 1 V are due to abrupt  $\Delta\varphi$  changes. The trends of the two curves match very well, indicating that the simulation method is correct. The intensity deviations are due to the simplification in our simulation, while the real conditions are complex. Even so, the method can

predict the trends of diffraction efficiency versus applied voltage and optimize the performance of LC gratings with alternate TN and PA regions.

#### 4. Conclusion

A simulation method for LC gratings with alternate TN and PA regions is proposed. The mechanism of this kind of grating is well explained. Simulation and analysis of voltage-dependent diffraction efficiency have been carried out. The experimental work presents good accordance with the simulation result, and diffraction efficiency increases evidently through our optimization. This method exhibits great potential for more complex photonics and display applications.

The authors are indebted to Prof. V. Chigrinov for his kind support with the photoalignment technique. This work is sponsored by 973 programs (Nos. 2011CBA00200 and 2012CB921803), the National Natural Science Foundation of China (No. 11304151) and Ph.D. Programs Foundation of Ministry of Education of China (No. 20120091120020).

#### References

1. X. W. Lin, W. Hu, X. K. Hu, X. Liang, Y. Chen, H. Q. Cui, G. Zhu, J. N. Li, V. Chigrinov, and Y. Q. Lu, "Fast response dual-frequency liquid crystal switch with photo-patterned alignments," *Opt. Lett.* **37**, 3627–3629 (2012).
2. S. R. Nersisyan, N. V. Tabiryan, D. M. Steeves, and B. R. Kimball, "Optical axis gratings in liquid crystals and their use for polarization insensitive optical switching," *J. Nonlinear Opt. Phys. Mater.* **18**, 1–47 (2009).
3. B. Apter, U. Efron, and E. Bahat-Treidel, "On the fringing-field effect in liquid-crystal beam-steering devices," *Appl. Opt.* **43**, 11–19 (2004).
4. W. M. Gibbons and S. T. Sun, "Optically generated liquid crystal gratings," *Appl. Phys. Lett.* **65**, 2542–2544 (1994).
5. X. K. Hu, B. Y. Wei, X. W. Lin, W. Hu, G. Zhu, V. Chigrinov, and Y. Q. Lu, "Complex liquid crystal alignments accomplished by Talbot self-imaging," *Opt. Express* **21**, 7608–7613 (2013).
6. R. L. Sutherland, V. P. Tondiglia, L. V. Natarajan, T. J. Bunning, and W. W. Adams, "Electrically switchable volume gratings in polymer-dispersed liquid-crystals," *Appl. Phys. Lett.* **64**, 1074–1076 (1994).
7. Y. Q. Lu, F. Du, and S. T. Wu, "Polarization switch using thick holographic polymer-dispersed liquid crystal grating," *J. Appl. Phys.* **95**, 810–815 (2004).
8. D. Subacius, S. V. Shiyankovskii, P. Bos, and O. D. Lavrentovich, "Cholesteric gratings with field-controlled period," *Appl. Phys. Lett.* **71**, 3323–3325 (1997).
9. Z. Zheng, F. Guo, Y. Liu, and L. Xuan, "Low threshold and high contrast polymer dispersed liquid crystal grating based on twisted nematic polarization modulator," *Appl. Phys. B* **91**, 17–20 (2008).
10. J. Yan, Y. Li, and S. T. Wu, "High-efficiency and fast-response tunable phase grating using a blue phase liquid crystal," *Opt. Lett.* **36**, 1404–1406 (2011).
11. G. Zhu, J. N. Li, X. W. Lin, H. F. Wang, W. Hu, Z. G. Zheng, H. Q. Cui, D. Shen, and Y. Q. Lu, "Polarization-independent blue-phase liquid-crystal gratings driven by vertical electric field," *J. Soc. Inf. Disp.* **20**, 341–346 (2012).
12. R. G. Lindquist, J. H. Kulick, G. P. Nordin, J. M. Jarem, S. T. Kowel, M. Friends, and T. M. Leslie, "High-resolution liquid-crystal phase grating formed by fringing fields from interdigitated electrodes," *Opt. Lett.* **19**, 670–672 (1994).
13. M. Bouvier and T. Scharf, "Analysis of nematic-liquid-crystal binary gratings with high spatial frequency," *Opt. Eng.* **39**, 2129–2137 (2000).
14. L. L. Gu, X. N. Chen, W. Jiang, B. Howley, and R. T. Chen, "Fringing-field minimization in liquid-crystal-based high-resolution switchable gratings," *Appl. Phys. Lett.* **87**, 201106 (2005).
15. B. Wen, R. G. Petschek, and C. Rosenblatt, "Nematic liquid-crystal polarization gratings by modification of surface alignment," *Appl. Opt.* **41**, 1246–1250 (2002).
16. J. Chen, P. J. Bos, H. Vithana, and D. L. Johnson, "An electro-optically controlled liquid crystal diffraction grating," *Appl. Phys. Lett.* **67**, 2588–2590 (1995).
17. W. Hu, A. K. Srivastava, X. W. Lin, X. Liang, Z. J. Wu, J. T. Sun, G. Zhu, V. Chigrinov, and Y. Q. Lu, "Polarization independent liquid crystal gratings based on orthogonal photoalignments," *Appl. Phys. Lett.* **100**, 111116 (2012).
18. W. Hu, A. Srivastava, F. Xu, J. T. Sun, X. W. Lin, H. Q. Cui, V. Chigrinov, and Y. Q. Lu, "Liquid crystal gratings based on alternate TN and PA photoalignment," *Opt. Express* **20**, 5384–5391 (2012).
19. V. G. Chigrinov, V. M. Kozenkov, and H. S. Kwok, *Photoalignment of Liquid Crystalline Materials: Physics and Applications* (Wiley, 2008).
20. S. Y. Huang, S. T. Wu, and A. Y. G. Fuh, "Optically switchable twist nematic grating based on a dye-doped liquid crystal film," *Appl. Phys. Lett.* **88**, 041104 (2006).
21. V. Kapoustine, A. Kazakevitch, V. So, and R. Tam, "Simple method of formation of switchable liquid crystal gratings by introducing periodic photoalignment pattern into liquid crystal cell," *Opt. Commun.* **266**, 1–5 (2006).
22. B. Y. Wei, W. Hu, Y. Ming, F. Xu, S. Rubin, J. G. Wang, V. Chigrinov, and Y. Q. Lu, "Generating switchable and reconfigurable optical vortices via photopatterning of liquid crystals," *Adv. Mater.* **26**, 1590–1595 (2014).
23. H. Wu, W. Hu, H. C. Hu, X. W. Lin, G. Zhu, J. W. Choi, V. Chigrinov, and Y. Q. Lu, "Arbitrary photo-patterning in liquid crystal alignments using DMD based lithography system," *Opt. Express* **20**, 16684–16689 (2012).